Int. J. Electrochem. Sci., 7 **(2012)** 445 - 470

International Journal of ELECTROCHEMICAL SCIENCE
www.electrochemsci.org

Comparison of Corrosion Resistance of Carbon Steel and Some Stainless Steels Exposed to LiBr-H_2O Solution at low Temperatures

C. Cuevas Arteaga[1,*], *J. Porcayo Calderón*[2], *C. F. Campos Sedano*[3], *J. A. Rodríguez*[1]

[1] Centro de Investigación en Ingeniería y Ciencias Aplicadas, Universidad Autónoma del Estado de Morelos. Av. Universidad 1001, Col. Chamilpa, Cuernavaca, Morelos, C.P. 62209, México. Tel 52(777) 3 29 70 84 Ext. 6233, Fax 52(777 3 29 79 84.
[2] Instituto de Investigaciones Eléctricas, Gerencia de Materiales y Procesos Químicos, Calle Reforma 113, Colonia Palmira, C.P. 62490, Cuernavaca, Morelos, México.
Tel 52(777) 362 38 11 Ext. 7262, Fax 52(777) 362 38 32.
[3] Facultad de Ciencias Químicas e Ingeniería, Universidad Autónoma del Estado de Morelos. Av. Universidad 1001, Col. Chamilpa, Cuernavaca, Morelos, C.P. 62209, México.
[*]E-mail: ccuevas@uaem.mx

Received: 4 November 2011 / *Accepted:* 13 December 2011 / *Published:* 1 January 2012

A corrosion evaluation has been made using the electrochemical current and potential noise technique (EN), polarization curves (PC) and conventional weight loss method (WL) to determine the corrosion performance of a carbon steel exposed to LiBr-H_2O (50% wt.) solution at 25, 60, and 80°C. From the noise measurements, the resistance noise (*Rn*) was determined, and then the Stern-Geary equation and Faraday's Law were applied to determine the mass loss. The mass loss obtained from EN after 15 days of exposure was compared to that obtained from WL, observing the same behavior with temperature. The electrochemical noise time series and the spectral noise impedance were used to analyze the changes in corrosion activity of carbon steel under the experimental conditions. SEM observations of the corroded samples indicated that the carbon steel suffered localized corrosion in a generalized way; these results were according to the pattern of noise signals. To support the corrosion behavior obtained from EN, EDS analysis of the corrosion products together with atomic absorption analysis of the corrosive solution containing the corrosion products were also made. A comparison of corrosion kinetics of several stainless steel together with that of carbon steel showed that carbon steel has some features that make it corrosion resistant compared to some stainless steel.

Keywords: Carbon steel, electrochemical noise, pitting corrosion, lithium bromide

1. INTRODUCTION

Absorption heat pumps/transformers are the only heat exchanger-recovery systems capable of increasing the waste heat temperature to make it useful in an environmental friendly way. Its main use is in operations where latent heat is discharged, especially in drying, evaporation and distillation unitary processes and in heat recovery of cooling plants. Some absorbent solutions have been reported as corrosive species in refrigeration systems [1]. These systems consist basically of a generator, condenser, evaporator, absorber and a heat exchanger. An evaporator absorbs heat at a low temperature and the condenser rejects the heat at a high temperature. Lithium bromide is primarily used for the absorption in liquid phase. Refrigeration technology takes advantage of the heat transfer that occurs. Lithium bromide-water solution is one of the most commonly used because of low cost, availability, safety, hygroscopic character, affinity for water vapor and non-volatility. The main disadvantage is its corrosivity and sometimes corrosion inhibitors are necessary to avoid materials damage [2–4]. Corrosion phenomenon in refrigeration units generates hydrogen gas that reduces the internal vacuum and decreases the operation efficiency. In addition, the corrosion products foul narrow openings in spray headers and heat exchanges [3].

Until now, it has been published several works about the corrosion of stainless steel caused by lithium bromide solutions [5-9], which have been frequently studied using the potentiodynamic polarization curves (PC) under limited temperature conditions. The utilization of the potentiodynamic polarization curves applying high potentials is important due to a basic knowledge about the corrosion mechanism and a general behavior of the material can be obtained. Through the PC technique, it is also possible to determine the corrosion potential, the current density, passivation and re-passivation regions, limit currents, etc., but it is not possible to obtain the corrosion kinetics, nevertheless, the polarization curves provide useful information to compare the corrosion resistance of different materials under the same experimental conditions. The electrochemical technique such as current and potential noise, besides providing the corrosion mechanism, provides the tools to determine the corrosion rate in time without perturbing the material. Recent works have been published where the electrochemical noise technique has been applied to determine the corrosion rates and type of corrosion of some stainless steel materials [10-17].

The objective of the present work was to obtain the corrosion kinetics during 15 days and determine the type of corrosion (general-pitting) of carbon steel exposed to lithium bromide aqueous solution (50 wt. %) at 25, 60, and 80°C, using the electrochemical noise technique, polarization curves, and the conventional weight loss method. Additionally, a comparison of corrosion kinetics of several stainless steel previously studied under the similar methodology than that applied to study carbon steel will be presented.

2. EXPERIMENTAL PROCEDURE

The corrosive solution was prepared with lithium bromide analytical grade regents and distilled water. LiBr was dehydrated in an electrical stove. 100 ml of corrosive solution was used for electrochemical tests and for the conventional weight loss method, introducing the corrosive solution

into an open flask, which was placed on an electrical stove obtaining the test temperature higher than the ambient temperature. Electrodes were made of a plate of low carbon steel, which composition was obtained from the spark analysis spectroscopy by triplicate obtaining the next average composition (wt.%):0.1714C-0.177Si-0.657Mn-0.0154P-0.0575S-0.22Cr-0.0733Mo-0.2064Ni-0.0196Al-0.0148Co-0.3581Cu-0.0027Ti-0.0059Pb-BalFe. Each sample was cut to size 2 mm x 4mm x 5mm and ground to 600 grit silicon carbide paper on all faces, rinsed with distilled water, degreased with acetone and dried under a warm air stream. For electrical connection, the specimens were spot welded to an 80Cr-20Ni wire, 150 mm long and 1.0 mm in diameter. Glass tubes were used for isolating the 80Cr-20Ni wire from the corrosive solution, and then the specimens were mounted in cross section and embedded in a polyester resin. The preparation of specimens, as well as the corrosive solution was the same for electrochemical noise measurements and potentiodynamic polatization tests.

For electrochemical potential and current noise (EN), the electrochemical cell was formed by a three identical electrodes setup. EN was simultaneously recorded with a sampling frequency of 1 Hz; 1024 measurements at each time series, which were obtained each four hours during 15 days. The polarization curves tests were made using an electrochemical cell constituted by the working electrode, a platinum wire as auxiliary electrode and an Ag/AgCl as the reference electrode. An over-potential from -500 mV to 1200 mV was applied to the electrochemical cell at a sweep rate of 1 mV/s. The over-potential was applied when a constant corrosion potential was obtained. Both techniques were performance through an ACM Gill AC potentiostat connected and controlled by a personal computer. In order to determine the amount of iron and some other possible elements dissolved during the corrosion process, the corrosion products contained in the corrosive solution from the EN measurements were analyzed by the atomic absorption technique, utilizing an Atomic Absorption Varian Spectrometer 220FS.

The weight loss technique (WL) was performed according to the ASTM Standards G1 [18] and G31 [19] using three different specimens. These specimens were also grounded to 600 grit silicon carbide papers on all faces, rinsed with distilled water, degreased with acetone and dried under a warm air stream. For the weight loss method, specimens in triplicate of the same size than that for electrochemical techniques were used. Before the immersion, the specimens were cleaned with acetone and weighted in an analytical balance Adventurer Ohaus model AR2114 with a precision of 0.0001g. After the immersion time, the specimens were cleaned from the corrosion products, and then weighted again in the same analytical balance. The difference between the initial and final weights divided between the initial areas was the mass loss. As it was explained before, the exposure was made by triplicate, and when the differences in weight loss at the final weighing was >10%, the test was repeated.

Specimens with corrosion products adhered to their surface after exposing to LiBr-H_2O solution applying EN, and the same specimens free of corrosion products were observed by mean of the Scanning Electron Microscopic (SEM) coupled with energy dispersive X-ray analyzer (EDX). Surface morphology examination of the corroded specimens and some quantitative analyses were made. SEM analysis was carried out through the Zeiss DSM 960 Microscopy.

3. RESULTS AND DISCUSSION

3.1. Physical Corrosion Characterization

Figure 1 present two images of the microstructure taken from SEM of carbon steel, which was obtained exposing the material during two minutes in a solution containing 10 ml of HNO_3, 15 ml of HCl, 10 ml of acetic acid and 5 drops of glycerin.

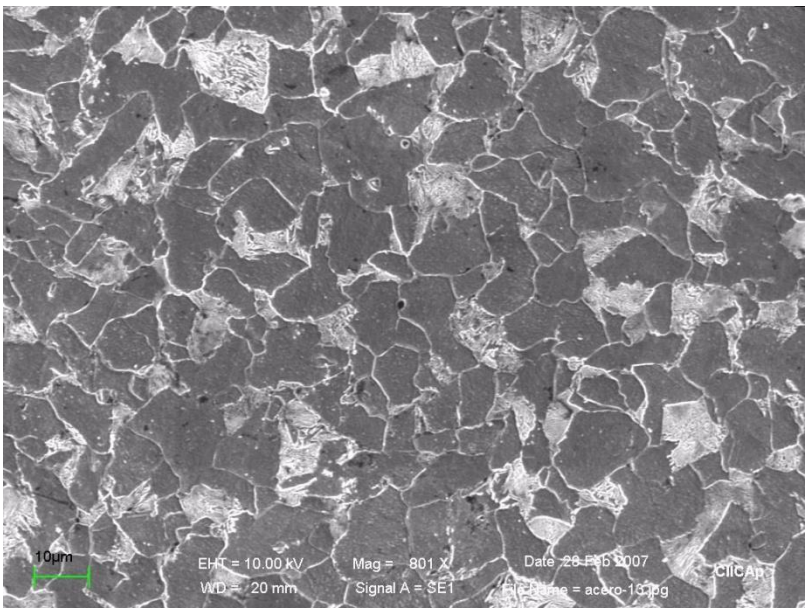

A

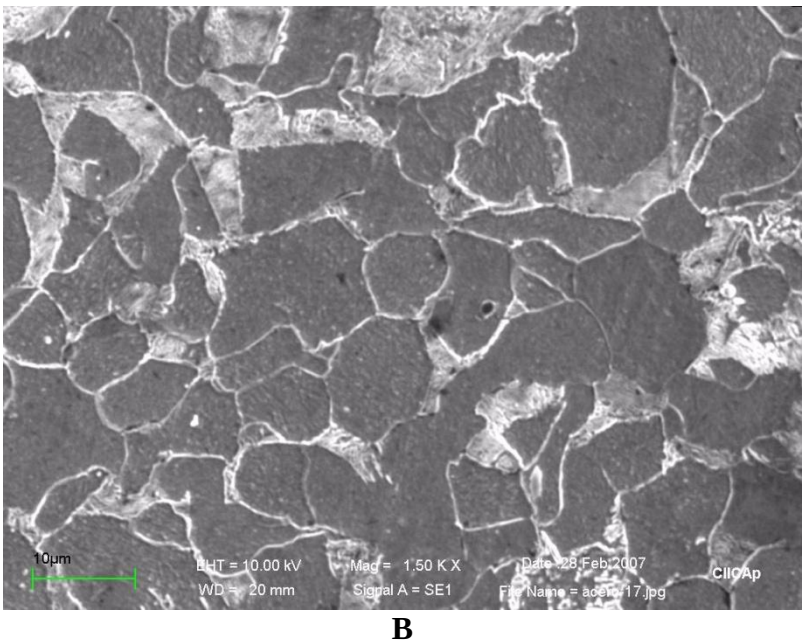

B

Figure 1. Optical images of the microstructure of carbon steel.

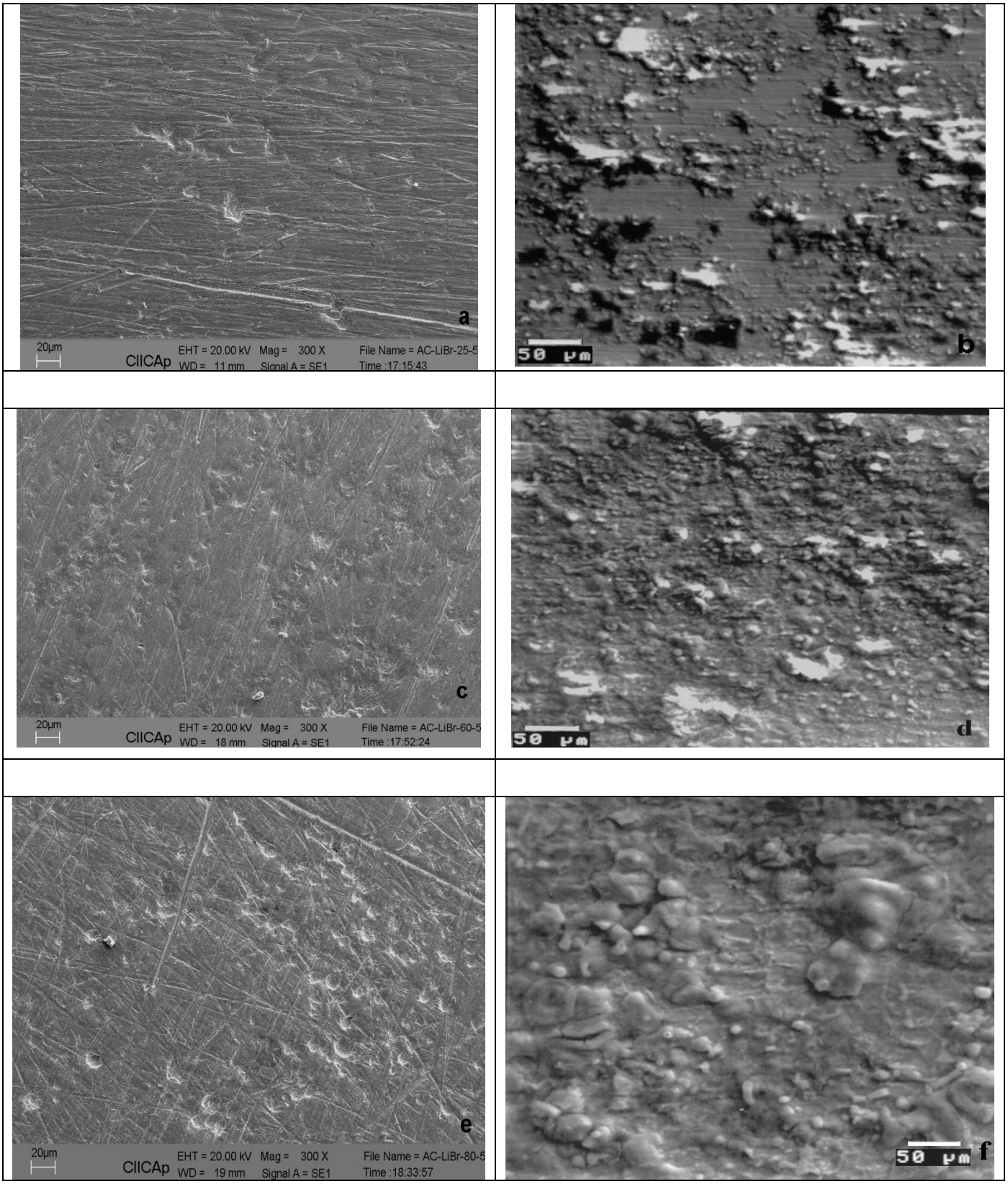

Figure 2. SEM images of corroded carbon steel after exposing 15 days in LiBr-H_2O solution in clean and with corrosion products, (a,b) 25°C, (c,d) 60°C, (e,f) 80°C.

This solution was chosen according to the standard ASTM E407-99 [20], revealing principally the grain boundaries of the steel. Such steels are hot rolled at elevated temperatures when they have an austenite (γ) crystal structure followed by relatively rapid cooling [21]. During the rapid cooling, the γ partially transforms to proeutectoid ferrite α, and the remaining γ transforms to pearlite, which leads to their microstructure of proeutectoid ferrite α plus pearlite as illustrated in Figure 1. The pearlite consists of ferrite interlaced with laths of cementite (Fe_3C). The microstructure at low magnification (800x) showed ferrite rich and pearlite rich areas. The pearlite was interconnected in the pearlite rich bands as shown in Fig 1b. Also, the microstructure presents isolated pearlite smaller compared to the interconnected pearlite. The isolated pearlite colonies mostly occurred at triple points or at α/α grain boundaries. The ferrite grain shape was irregular, with a grain size about 10 μm. Most of ferrite grain boundaries were curved as shown in Figure 1. This is a ferrite microstructure corresponding to carbon steel with an amount in carbon less than 0.6%, which is the case of the carbon steel studied in this work. The cementite phase in carbon steel is hard and fragile, which could be the most susceptible to corrosion, especially in localized form, such as it will be seen through the SEM images resulting from the carbon steel exposed to LiBr-H_2O solution after 15 days, which are presented in Figure 2.

Figure 2 shows six electron images of the corroded carbon steel at all the test temperatures in their clean and with corrosion products conditions after exposing to BrLi-H_2O solution during 15 days applying the electrochemical noise technique at 25, 60 and 80ºC. The morphological pattern of the corroded carbon steel surfaces is alike at all test temperatures, observing several pits through the samples and having an increment in the pitting density with temperature. The pits size is variable, starting from 2μm to 20 μm. There are cathodic areas around the pits, which show scratches from the polishing process. Also, from the Figures 2b, 2d and 2f, it is observed that the sample at 25 ºC presents smaller amount of corrosion products than that at the higher temperatures, observing some free corrosion products areas. Whereas at 60 and 80 ºC all the metallic surface is covered by corrosion products. Apparently, at the lowest temperature, corrosion was not so severe, and the carbon steel generated low amount of corrosion products, which were produced as chemical interactions between the metallic cations from the oxidation reaction and oxygen from the aqueous solution. The areas covered by corrosion products at 25 ºC were that which suffered breakdown of the passive layer generating some isolated pits. At 60 and 80°C a more uniform passivation layer covers the total area of the samples, and additionally at 80 º C the layer appears thicker. In order to quantify the amount of corrosion products in each corrosive system, atomic absorption analysis (AA) were made, which results are in agreement with the SEM morphology presented in Figure 2. The AA results will be presented later. Figure 3 presents an energy dispersion spectrum of the corrosion products of the carbon steel studied under the test conditions at 25ºC; similar spectrums were obtained at the higher temperatures. The spectrum shows a great amount of iron and bromide, as an evidence of the formation of iron oxide as a primary corrosion product and iron bromide as a secondary corrosion product. Observing the micrographs before cleaning (with corrosion products), it can be seen that at 60 and 80ºC, the corroded surfaces contain a significant amount of corrosion products covering the total surface as it was said, which also indicates that corrosion process is thermally activated. This behavior indicates the susceptibility of carbon steel when it is exposed to 50 (wt. %) aqueous lithium bromide

solution to suffer pitting corrosion, especially when temperature is increasing, as it has been evidenced by means of SEM.

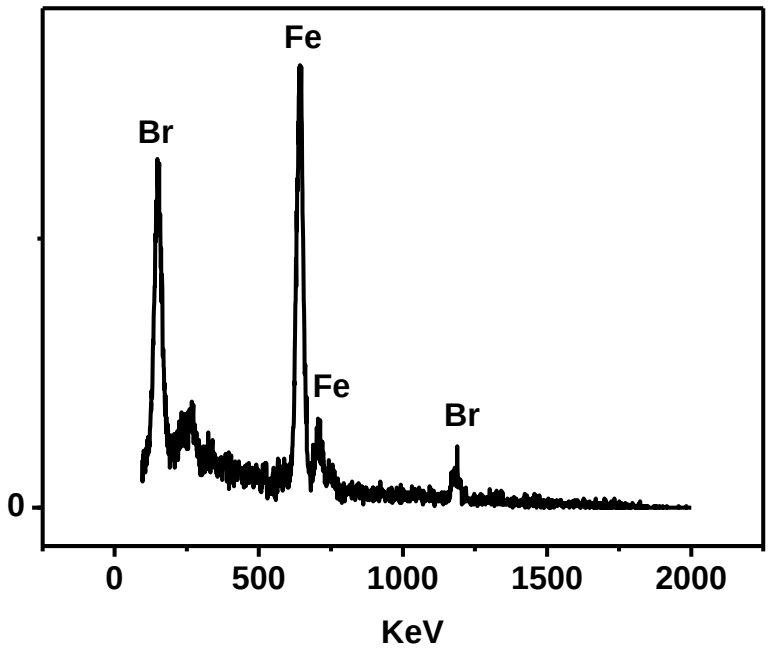

Figure 3. EDS analysis of the corrosion products.

3.2. Potentiodynamic Polarization Curves

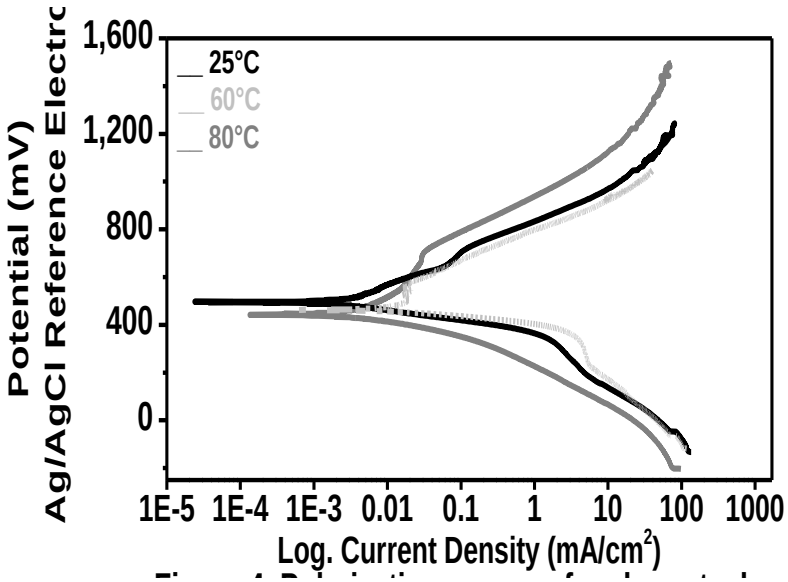

Figure 4. Polarization Curves of Carbon Steel.

Figure 4 shows the potentiodynamic polarization curves at all the studied temperatures. These plots show that corrosion potentials (E_{corr}) are very close each other, became more active with

temperature. E_{corr} was in the positive range from 447.0 mV at 80 ºC to 490.0 mV at 25 ºC, being 459 mV for 60 ºC (Ag/AgCl reference electrode). Some others LiBr-H_2O (50 wt. %) systems have been studied evaluating the corrosion performance of SS-316 and SS-316L stainless steel [14,15], in which the behavior of E_{corr} have shown that in general E_{corr} is more active with temperature, and in another materials such as SS-304 and SS-304L [10,12,22], E_{corr} has had an opposite behavior. Probably, there is a significant effect of the concentration of some other elements such as chromium, nickel, molybdenum or magnesium on corrosion reactions and corrosion mechanisms. The temperature had an effect over the corrosion activity of the material, condition that was also observed in corrosion rates from electrochemical noise, as it will be presented later. At 60°C there was a current density limit of 0.03 mA/cm^2 observed approximately between 500 and 600 mV. This behavior can be related to the corrosion products formed. A current limit indicates that the material formed a corrosion products layer over its surface protecting itself and keeping the current density constant. Afterward, there is an active plot, where an increase in the corrosion current density from 0.03 to 70 mA/cm^2 is seen, which evidence the susceptibility of carbon steel to corrode under LiBr-H_2O solution. At 25 and 80°C, the anodic curves showed only an active process, having a similar behavior, observing two different slopes, as well as at 60°C; the first one with a change in current with potential relatively small compared to the second one, as an evidence of the changes suffered by the oxides film over the metallic surface. With the exception of the current limit presented at 60°C, the anodic branches at the three temperatures are similar, indicating that the corrosion mechanisms in all the cases is alike, with the difference in the severity in pitting with temperature, such as is evidenced in Figure 2. From the polarization curves some parameters such as E_{corr}, the corrosion density and the Tafel slopes were obtained applying the Tafel extrapolation method (see Table 1).

Table 1. Parameters obtained from the Polarization Curves at all the test temperatures

Temperature (°C)	25	60	80
ba (mV/dec)	112	134	143
bc (mV/dec)	62	52	60
E_{corr} (mV)	490	459	447
I_{corr} (mA/cm^2)	3.16E-3	3.45E-3	3.78E-3

As it can be seen, the current density is becoming higher with temperature, which is in accordance with the values of E_{corr} and the corrosion rates determined from electrochemical noise. For the present study, the polarization curves are important because the anodic and cathodic slopes *ba* and *bc* were determined to be used in the calculation of corrosion rates from the electrochemical noise through the resistance noise *Rn*, using the Stearn–Geary equation. The Tafel regions in the polarization curves are not well defined, probably reflecting the importance of mass-transfer conditions, especially *ba*, where the Tafel slopes were the largest values, indicating that the diffusion of the species can have an influence on the rate controlling step. Tafel slopes lower than 100 mV/dec are typical for activation controlled systems, whereas Tafel slopes with larger values are typical for systems which are not

purely activation or diffusion controlled [23,24]. The cathodic branches are analogous at all temperatures, with a tendency to a limit current, which will be associated to oxygen diffusion. In general, the cathodic curves pattern at all temperatures indicated the reduction reactions of both: hydrogen ions and oxygen, hence the lithium bromide solution has a pH of 5.4 and species of hydrogen and oxygen are present to participate in reduction reactions [14].

3.3. Electrochemical Noise Technique

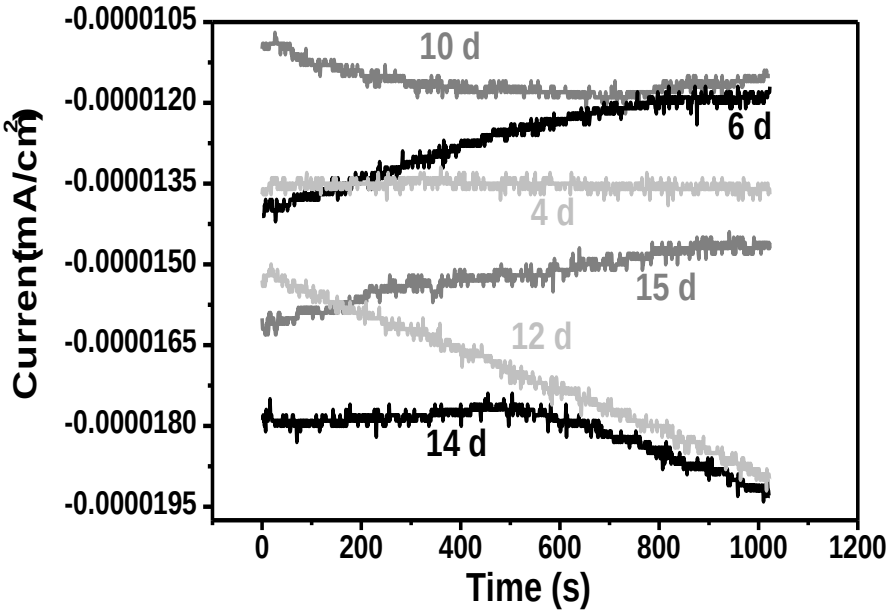

Figure 5. Current time series of carbon steel at 25°C.

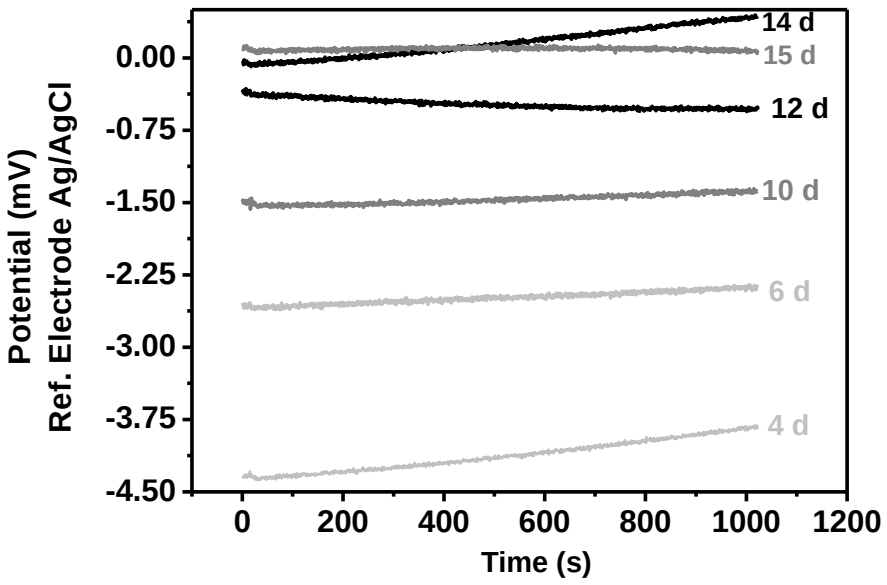

Figure 6. Potential time series of carbon steel at 25°C.

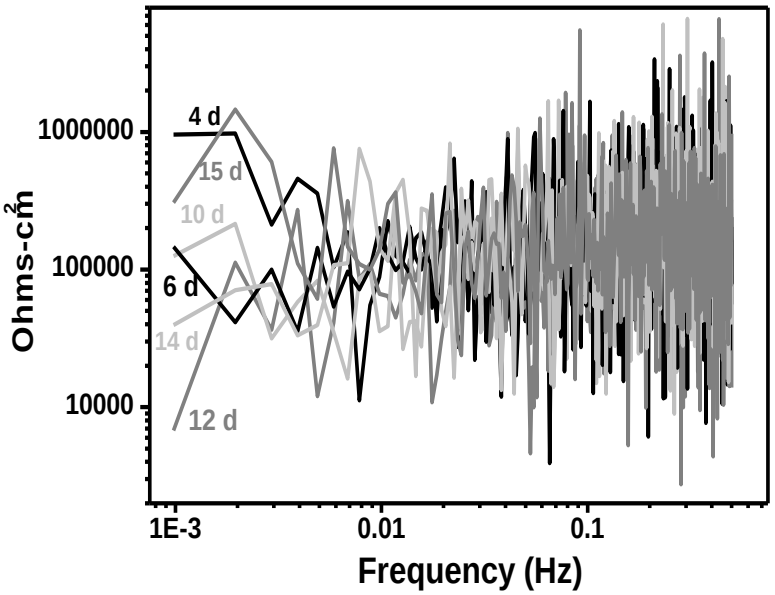

Figure 7. Spectral impedance of carbon steel at 25ºC

It is important to point out that even thought for each study temperature approximately 90 time series in current and potential were simultaneously measured, in this section will only be presented some current times series and their corresponding potential time series, which is due to the noise signals were similar along the experiments. Figures 5-7 show the electrochemical current density and potential noise signals, and the impedance spectrum at different times of immersion (4, 6, 10, 12, 14 and 15 d) for carbon steel at 25°C exposed to LiBr-H_2O solution (50% wt). The spectral noise impedance (SN) plots were obtained using an algorithm based on the Fast Fourier Transform (FFT) of spectral analysis. The resolved frequency bandwidth of interest lies between 0.1 and 500 mHz. The electrochemical noise time series and the spectral noise impedance were used to analyze the changes in corrosion activity of carbon steel under the experimental conditions. At 25ºC, the current time series present some medium intensity anodic/cathodic transients together with stochastic oscillations in a sequential way, within a current density between $-1.05x10^{-5}$ to $-1.95x10^{-5}$ mA/cm^2. Also, it is seen that current values are negative, which indicates that the second working electrode was acting as the anode electrode [25]. In general, the current density tended to increase in time, and the transients were intensified during the last days of the test period (See time series at 12, 14 and 15 days), thus, it is possible that the pits resulting at 25ºC, were formed at the end of the immersion time. The potential time series present a high level noise, nevertheless the values keep almost constant, observing that potential becomes nobler with time. The noise spectra as a function of time obtained present constant "white noise" impedance in the frequency bandwidth considered (independent of frequency). The overall noise impedance decreased with time of immersion from 1×10^6 Ω.cm^2 to 7×10^3 Ω.cm^2 at low frequency, indicating that corrosion rate increase in time, which is in agreement with the behavior of corrosion density obtained from the current time series. This behavior suggests that the material protected during the first days, forming an adhered and coherent film over the surface, which suffered a breakdown or the nucleation of pits. At the last days of the experiment, it is stated the presence of a

porous and a less protective condition of the corrosion products layer, such as it could be seen through the micrographs at this temperature (Figure 2.b).

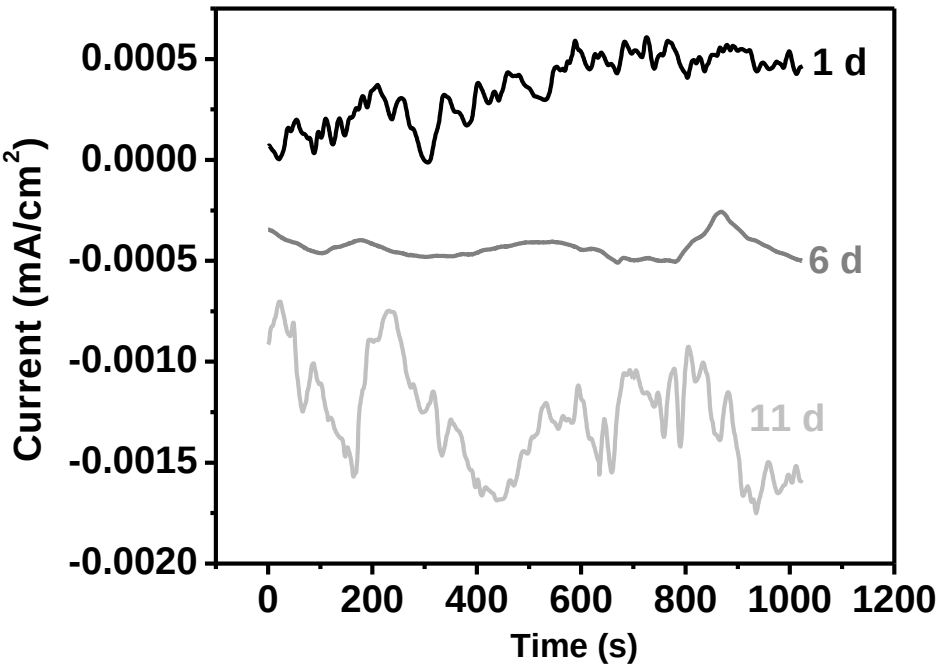

Figure 8. Current time series of carbon steel at 60°C.

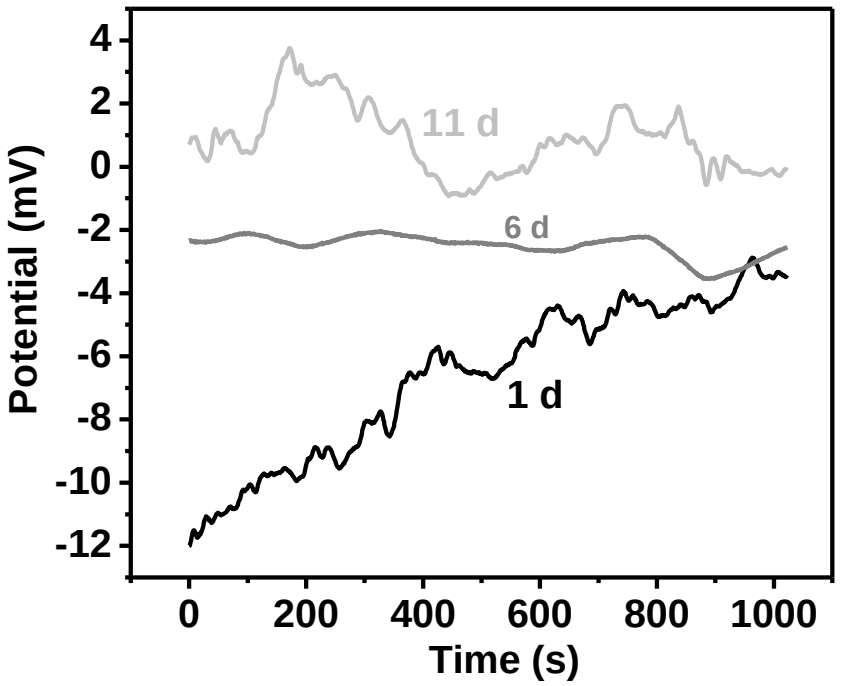

Figure 9. Potential time series of carbon steel at 60°C.

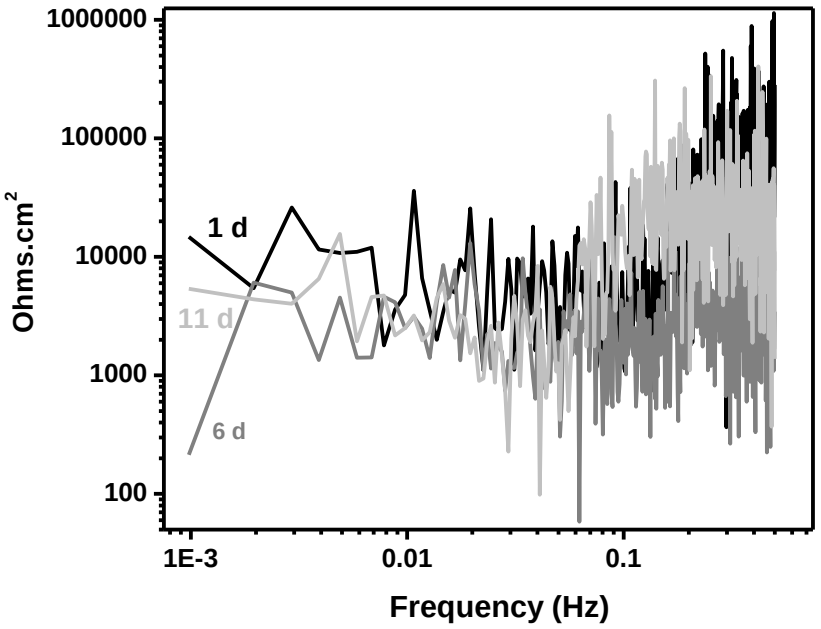

Figure 10. Spectral impedance of carbon steel at 60ºC

Figures from 8 to 10 show the electrochemical current density and potential noise signals, and the impedance spectrum at different times of immersion for 60°C (1, 6 and 11 d). The noise pattern of all the current time series is the same, showing low intensity and high frequency noise. There are no transients, and the noise is the so called "white noise". The current values are positive and negative; also observing that sometimes each of the working electrodes performs as the anode and the cathode. The current density is increasing in time (absolute values of current density) from 5 x 10^{-4} to 1.17 x 10^{-3} mA/cm^2, magnitudes higher than that at 25°C, which is in agreement with E_{corr} and I_{corr} obtained from the potentiodynamic polarization curves. With respect to the potential times series, their behavior is according to the current pattern, in the sense that there are no transients, showing high frequency and low amplitude transients. The results from electrochemical noise is not reflecting the results of the pitting morphology of samples, hence the importance of making a visual observation of samples and a statistic analysis from the electrochemical noise, which will be presented later. The noise impedance spectra are similar to that observed at 25ºC, where the impedance is independent of frequency, observing that the impedance decreased in time. The range of impedance at low frequency was from 200 Ω.cm^2 to 20000 Ω.cm^2, magnitudes lower than that at 25°C, which means that the corrosion density is higher at the higher temperature, which is in agreement with E_{corr} and I_{corr} from the polarization curves and the current time series.

Figures 11 through 13 present the electrochemical current density and potential noise signals, and the impedance spectra at different times of immersion for 80°C (2, 3, 5 and 14 d) for carbon steel exposed to LiBr-H_2O corrosive solution (50% wt.). The current noise-time records seem to have similar characteristics: low-amplitude, high-frequency stochastic oscillations accompanied with some significant transients, especially at 2 and 5 d, where the largest intensity of the transients was 1.125 x

10^{-5} mA/cm^2 at 2d. These transients are evidence for the nucleation of localized sites and/or the rupture and recovery of the passive film.

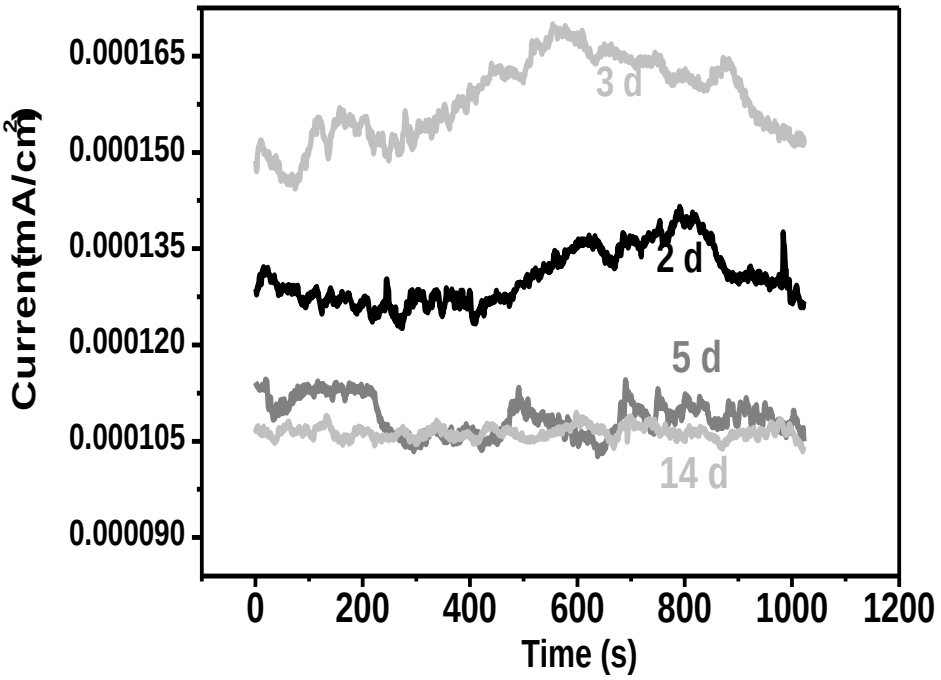

Figure 11. Current time series of carbon steel at 80°C.

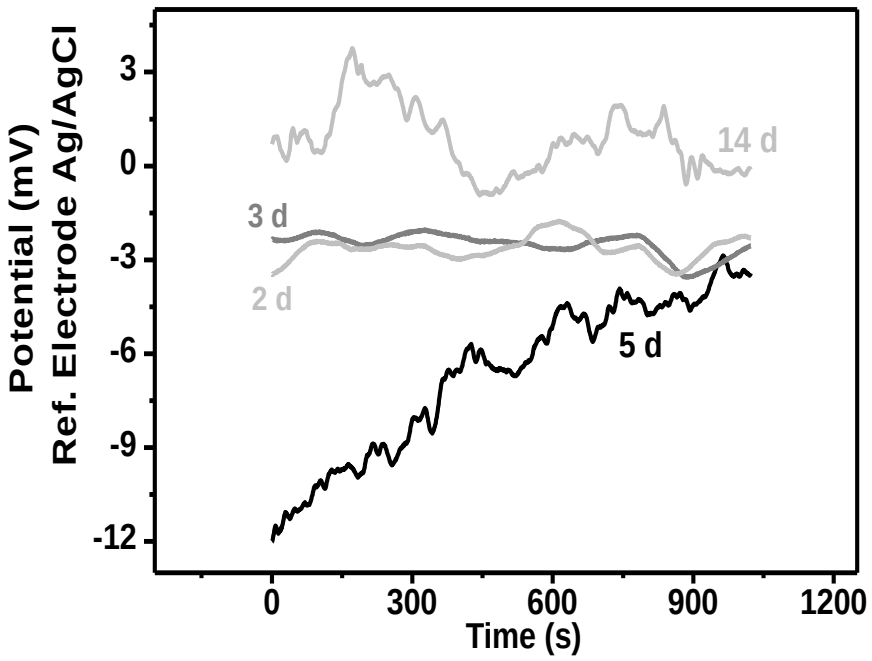

Figure 12. Potential time series of carbon steel at 80°C.

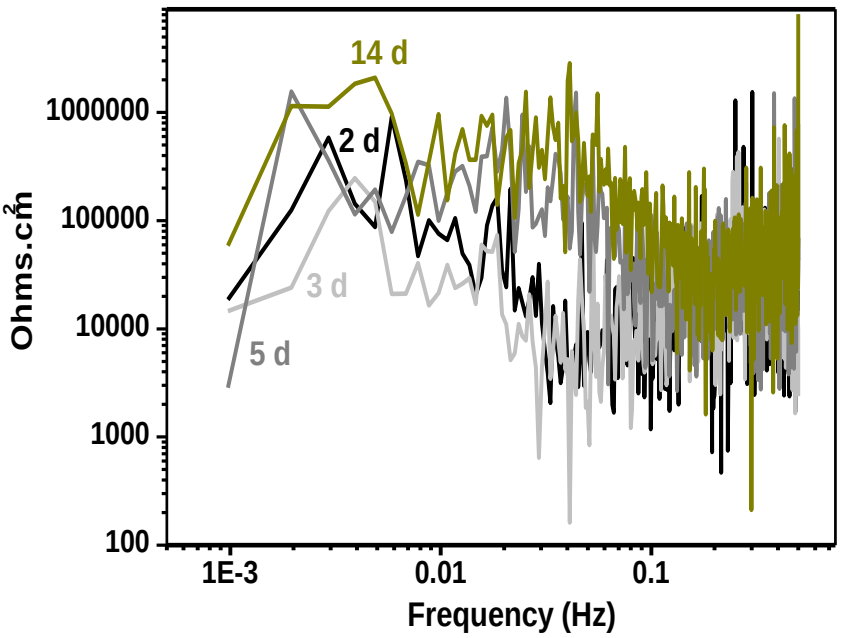

Figure 13. Spectral Impedance of Carbon Steel at 80°C

The low-amplitude, high-frequency stochastic oscillations also evidence a uniform corrosion process. The current density had an oscillatory behavior increasing at the beginning of the immersion, and decreasing afterward. The current density values were all positive, from 1.05 x 10^{-4} to 1.72 x 10^{-4} mA/cm^2, magnitudes similar to those at 60ºC. The tendency of the current density to decrease in time is a result of the protection of the material forming a thick and coherent Fe_2O_3 oxide layer, such as was observed by means of SEM (See Figure 2.f) after finishing the experiment, and by means of EDS analysis and atomic absorption results (presented later). It is interesting to note that the thickness of the metallic oxide formed over the surface at 80ºC is not uniform, which can be due to the microstructure of the studied carbon steel is a proeutectoid ferrite α plus pearlite, in which the pearlite consists of ferrite interlaced with laths of cementite (Fe_3C), a hard and fragile phase susceptible to corrosion, especially in localized form at this temperature. It is possible that the thinner metallic oxide layer be more susceptible to be broken by the effect of the corrosive species to produce pits nucleation. At 3 and 14 days there are also some transients of lower amplitude than that at 2 and 5 days. At 14 d there was less corrosion activity; hence the oscillations appeared to be of lower intensity and the current magnitude was lower than at the others times. From the above analysis, it can be said that oscillations and transients of electrochemical measurements are associated with a continuous change of metal surface due to the exposure to LiBr-H_2O solution, and it can be inferred that carbon steel suffered a kind of generalized corrosion with localized events and the rupture and recovery of passive film, behavior confirmed with the visual observations from SEM analysis (Figure 2.e). With respect to the electrochemical potential records, for 2 and 3 d immersion periods, the potential noise exhibited some lower frequency drift, which disappeared afterward. In general, potential time series have low amplitude, high-frequency stochastic oscillations with no transients, which have no good correspondence with current time series. The open-circuit potentials were between 3 mV and -12 mV

(Ag/AgCl reference electrode), observing an increase of potential with time, which indicates the formation of a passive film, such as the current density time series indicated, and was observed from the SEM image.

The spectral noise impedance showed that at low frequencies the amplitude impedance was decreasing in time until 5 d, after that the amplitude increased. The magnitude of noise impedance along the bandwidth was from 150 to 8 x 10^6 $\Omega.cm^2$, observing the variable low frequency impedance values obtained from 3000 to 60000 $\Omega.cm^2$. Also, it is seen that at the first 5 days the noise impedance decreased and then increased, which suggest an active condition at the beginning of the immersion and a passive condition afterward. Impedance spectra obtained for different times of immersion present similar differences in slope. At the very low frequency, the behavior is a shallow slope, then a slope from 0.04 to 0.2 Hz for 5 and 14 days, and from 0.02 to 0.06 Hz for 2 and 3 days is observed, after that and until the very high frequency, there are shallow slopes for all the times immersion. This cyclic behavior means that the significant transients obtained from the electrochemical noise are alike in magnitude, then the noise magnitude decreases in frequency until making frequency independent, which could indicate that the corrosion phenomenon is repetitive along the immersion time, presenting pits of similar size and depth together with a generalized corrosion process, such as it is observed throughout the sample in Figure 2.e.

To corroborate the behavior of electrochemical noise signals about the corrosion process, the localization index LI was calculated as the ratio between the current noise standard deviation σ_i over the root-mean-square current value I_{rms} [26,27], which can be presented as indicator of localized corrosion activity. The analysis took into account the different ranges of LI values, which lie between 0 and 1. For current fluctuations, which are large compared to the mean current, LI will have values close to 1, while for current fluctuations, which are small compared to the mean current, LI will be close to 0 [28,29].

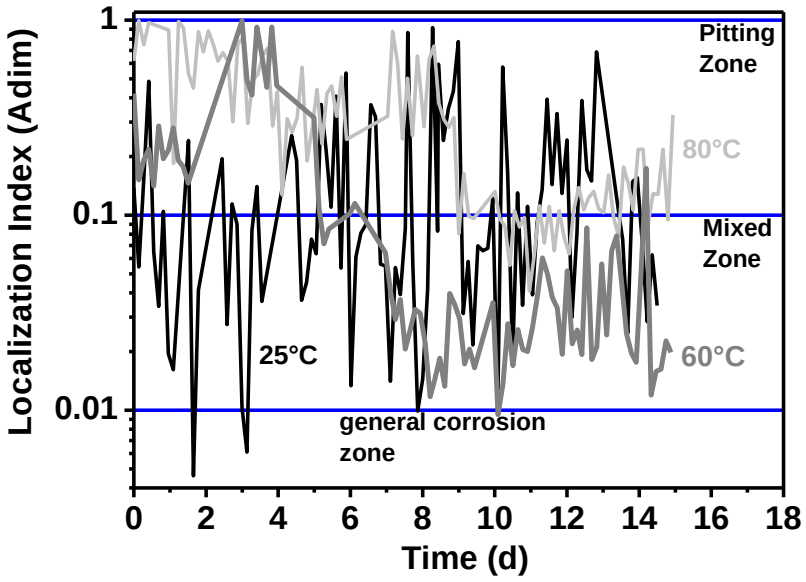

Figure 14. Localization index of carbon steel.

Figure 14 presents the localization index of carbon steel at the three test temperatures. LI values were obtained from every time series records throughout the exposure time. The localization indexes lie mostly in the zones of pitting and mixed values, being in a range of 0.01-1.0. At 25°C, most of the LI values are in the mixed zone until the 4th day of the experiment, and then, LI values lie generally into the pitting corrosion zone. A pitting corrosion process provokes a higher corrosion current density, therefore, the behavior of the current density from the electrochemical noise together with the intensification of the transients at 25ºC are in agreement with LI values. At 60°C, until the 5th day the localization indexes lie in the pitting zone, decreasing immediately to the mixed zone until the end of the experiment. It is important to notice that the current and potential time records did not reflect evidence of localized corrosion at this test temperature, nevertheless, the calculation of localization index, somehow indicates the presence of a localized corrosion process, which is in according with visual observations from the SEM micrograph (Figure 2.c), which shows several dispersed low depth and small size pits. At 80°C, the corrosive activity began in the pitting zone, decreasing with time until reaching the general corrosion zone at 10th day to increase almost immediately at the 12th day once again to the pitting zone. This behavior is in agreement with the current time series and SEM images for the higher test temperature, where important transients were presented and larger and deeper pits were observed.

3.4. Noise Resistance Rs and Mass Loss

A statistical analysis was made to the current and potential data to obtain the resistance noise *Rn* [28-30], which was calculated as the ratio between the potential standard deviation and current standard deviation. To convert the resistance noise ($\Omega.cm^2$) to corrosion current density I_{corr} (mA/cm^2), the Stern-Geary equation (Eq. 1) and Tafel equation (Eq. 2) [31-33] were used. The Faraday´s Law (Eq. 3) was also used to obtain the mass loss from I_{corr} electrochemical data.

$$I_{corr} = \frac{B}{Rn} \qquad \text{Eq. [1]}$$

Where B is related to the Tafel slopes as follows:

$$B = \frac{b_a b_c}{2.303(b_a + b_c)} \qquad \text{Eq. [2]}$$

Applying the Faraday´s Law, where the mass loss M, is given in $g/cm^2 min$:

$$M = K\, I_{corr}\, (EW) \qquad \text{Eq. [3]}$$

EW is the equivalent weight given by:

$$EW = \frac{1}{\sum \frac{n_i \ f_i}{AW_i}} \qquad \text{Eq. [4]}$$

Where n_i is the number of transferred electrons during oxidation process for each element $_i$ of the alloy. Being this material carbon steel, which composition is mainly iron; no having more than 2% (wt.) of another element, the value of *EW* was calculated considering only the data of the iron. The Tafel constants B from equation 2 were determined from the Tafel slopes obtained from the experimental polarization curves (See table 1). To calculate the overall mass loss at each day, it was necessary to integrate the six corresponding data for each day. This was done making an integration of the data multiplied by the interval time at which the resistance noise (time series) was taken (Eq. 5). The corrosion rates obtained from electrochemical measurements are shown in Figure 15.

$$Mday = \sum_{i=1}^{6} M \Delta t \qquad \text{Eq. [5]}$$

It is important to mention that the applications of this method must be considered as an approximation of the corrosion rate, since, on the one hand the Faraday´s Law assumes that uniform corrosion must be occurring, and on the other hand the Stern-Geary equation is pertinent when corrosion reactions are activation controlled.

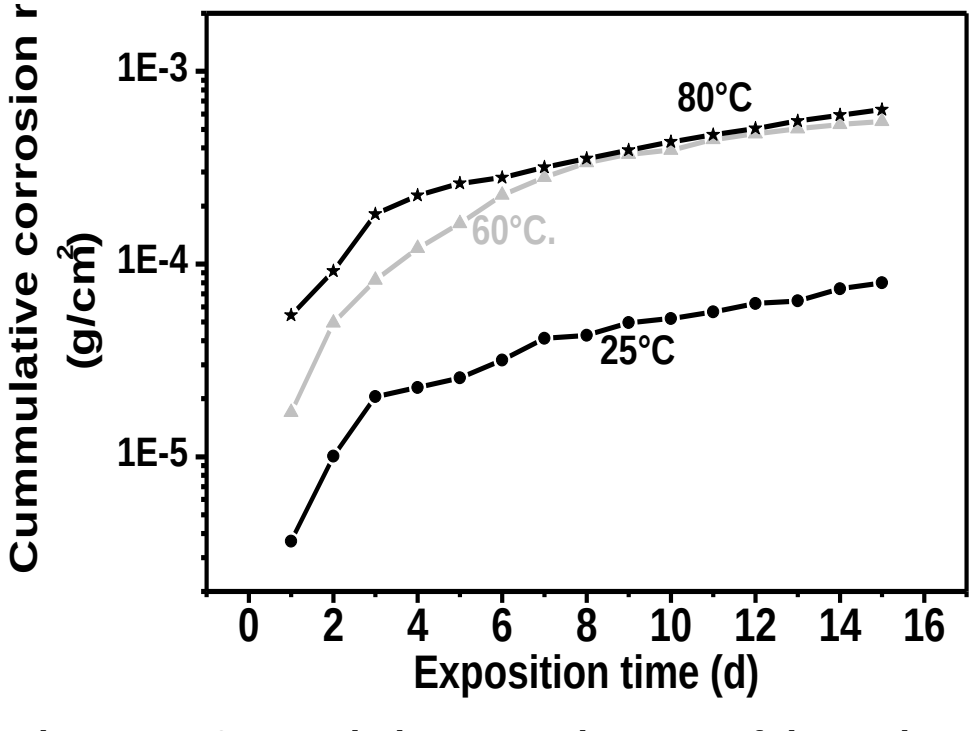

Figure 15. Cumulative corrosion rate of carbon steel

Nevertheless, some authors have reported good features in using the EN in corrosion research, indicating that the spontaneous fluctuations in current and voltage are normally sufficiently small (as it seems to be in the present system), that the constraints of linear system theory are satisfied [32]. Owing to the above exposed, to obtain a major certainty in the performance of carbon steel, the WL method has also been applied, which results will be shown next, together with the EN results.

The cumulative corrosion rate at all the test temperatures show that corrosion rates increased with temperature, and keep almost the same slopes along the immersion time, as evidence that corrosion process is alike at all the three temperatures, underlining that being a thermal process, the corrosion rate is higher at the higher temperatures. In addition, at 80°C the corrosion rate is the highest one until the 7th day, after that, corrosion rate was similar to that at 60 °C. Corrosion rate at 25ºC was lower one order of magnitude with respect to the two higher test temperatures. In general, corrosion rate is reaching constant values in time, showing that carbon steel is capable to protect itself. From this result, it can be said that in general, corrosion process was thermally activated. The fact that corrosion rate is almost the same at 60 and 80ºC from the 7th day can be explained from the point of view of the thermodynamics. Given that, it is known that the aqueous lithium bromide solution at 80°C suffers crystallization, phenomenon clearly seen when the experimental test was made. This crystallization produces a smaller amount of lithium bromide dissolved in the solution, therefore the concentration of the oxidant species Br was lower with respect to the corrosive solution at the other test temperatures, resulting in a corrosion rate similar to that at 60°C during the last eight days. This behavior was confirmed with the polarization curve at 80°C, in which the corrosion potential appears similar to that at 60ºC.

Table 2. Corrosion rates after 15 days for carbon steel calculated from electrochemical noise and weight loss method at the test temperature.

Exposure Temperature (°C)	Electrochemical Noise Technique (g/cm^2)	Weight Loss Method (g/cm^2)
25	0.8E-4	0.68E-3
60	5.48E-4	1.73E-3
80	6.32E-4	2.42E-3

A comparison of the mass loss calculated from electrochemical measurements and the conventional weight loss method for 15 days of exposure is presented in Table 2. From the conventional weight loss method, the mass loss resulted higher than that obtained from the electrochemical noise technique. This difference may be due to the uncertainty of very low values of mass loss generated in very small specimens in the weight-loss method. Other explanation could be the implications in the use of the Faraday´s Law and the Stern-Geary equation (to convert electrochemical data in mass loss), which assume that uniform corrosion is occurring and the corrosion reactions are activation controlled. Given that uniform corrosion was not seen in the corroded samples, and the Tafel regions in the polarization curves was not well defined, some errors could be introduced in the

calculation of the mass loss. Nevertheless, it is important to note that this difference was small, observing a difference of one order of magnitude.

3.5. Absorption atomic results

In order to determine the concentration of iron and other elements containing the carbon steel dissolved in the corrosive solution during the corrosion process at each test temperatures, the corrosive solutions were analyzed by the atomic absorption technique.

Table 3. Concentration obtained from the atomic absorption analysis of Fe present in the corrosion products contained in the LiBr solution after exposing the carbon steel at the different test temperatures.

Temperature (°C)	Concentration of Iron (ppm /100 ml)
25	17.5
60	242.7
80	480.8

According to the range of concentrations obtained of iron in the corrosive solution after the tests, which were from 17.5 to 480.8 ppm/100 ml (See table 3), the wave length utilized for the atomic absorption spectrometer was 248.3 nm for iron. The atomic absorption analyzer was a Varian 220 FS spectrometer, for which during the analyses a mixed gases of nitrous oxide and acetylene was used. The results of the absorption analysis demonstrated an increment of the concentration of iron with temperature. This behavior was also seen in the results of the corrosion rates from the electrochemical noise measurements. It was not possible to obtain some concentration of the other elements present at low concentration in the carbon steel.

3.6. Comparison of corrosion kinetics of carbon steel and some stainless steels.

Similar studies of several stainless steel have been made and reported elsewhere [10-17). The study of these materials was in an analogous way than the presented here for carbon steel. Kinetics corrosion at 15 days for stainless steel AISI-316 (UNS-S31600), AISI-316L (UNS-S31603), AISI-304 (UNS-S30400) and Carbon Steel; and corrosion kinetics at 10 days for stainless steel AISI-310 (UNS-S31000), AISI-310H (UNS-S31009), and AISI-321H (UNS-S32109) obtained after exposing to LiBr-H_2O solution (50% wt.) at 25, 60 and 80ºC is presented in Figures from 16 to 18. The material which presented the lowest corrosion rate at 25ºC was AISI-304, followed by AISI-310H, AISI-310, AISI-321H, carbon steel, AISI-316L, and the highest corrosion rate was for AISI-316. At 60 and 80ºC, AISI-310H presented the lowest corrosion rate, and AISI-304 incremented its corrosion rate with temperature in a significant way, nevertheless, carbon steel always had the major corrosion rate with respect to that obtained for AISI-304, AISI-310, AISI-310H and AISI-321H, but lower corrosion rate

with respect to AISI-316 and AISI-316L. The lower corrosion rate obtained for AISI-310H related to AISI-310 is due to the lesser contain of carbon presented for AISI-310H, since the composition of the rest of the alloying elements is identical (See Table 4 where the composition of the materials mentioned here is presented).

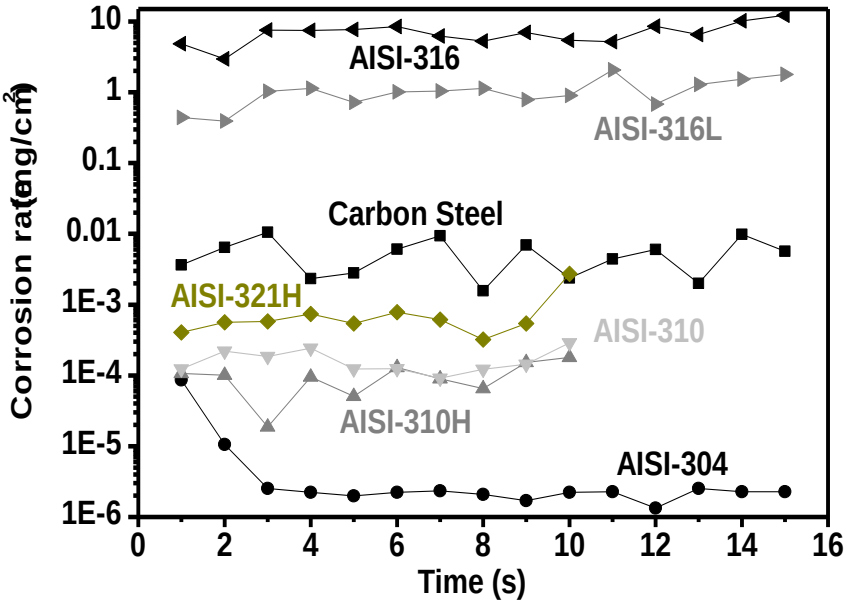

Figure 16. Comparison of the corrosion rate of some stainless steel materials and carbon steel exposed to LiBr-H_2O (50% wt) at 25ºC.

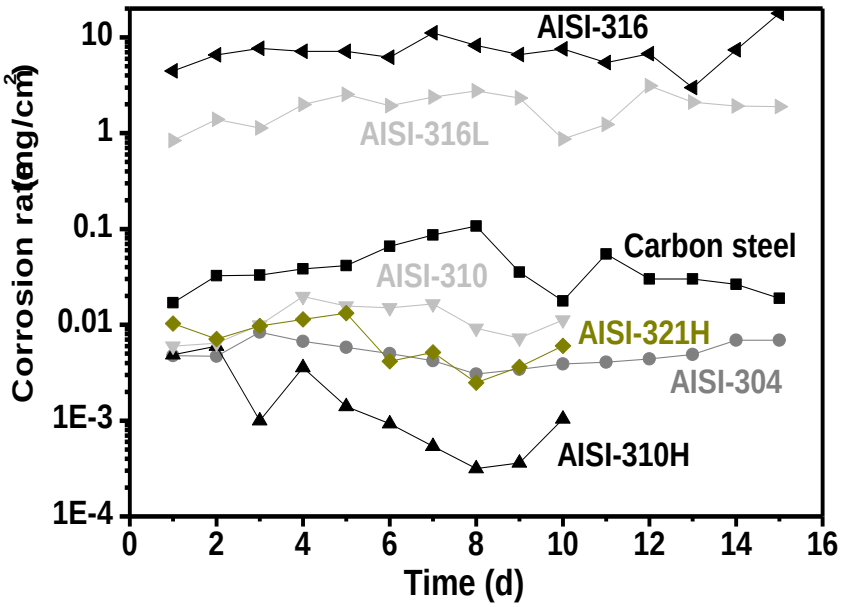

Figure 17. Comparison of the corrosion rate of some stainless steel materials and carbon steel exposed to LiBr-H_2O (50% wt) at 60ºC.

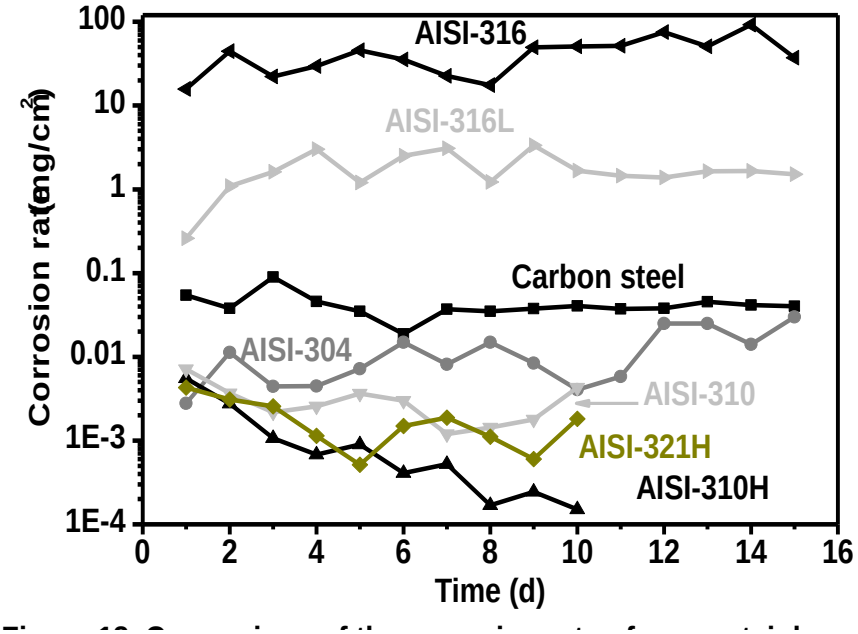

Figure 18. Comparison of the corrosion rate of some stainless steel materials and carbon steel exposed to LiBr-H_2O (50% wt) at 80ºC.

Table 4. Nominal composition of some studied materials under LiBr conditions (wt. %).

Materials	Fe	C	Cr	Ni	Si	Mn	P(max)	S(max)	Mo	Other
Carbon Steel	98.02	0.1714	0.22	0.2064	0.1777	0.657	0.0154	0.0575	0.0733	See Exp. Procedure
AISI-316	70.595	0.08 max	17	12	0.75	2.0	0.045	0.03	2.5	N 0.1 max
AISI-316L	70.544	0.03 max	17	12	0.75	2.0	0.045	0.03	2.5	N 0.1 max
AISI-304	69.34	0.08 max	19	8.75	0.75	2.0	0.045	0.03		
AISI-310	50.67	0.25 max	25	20.5	1.5	2.0	0.045	0.03		
AISI-310H	50.85	0.07	25	20.5	1.5	2.0	0.045	0.03		
AISI-321H	68.6	0.07	18	10.5	0.075	2.0	0.045	0.03		Ti 0.7 max N 0.1 max

It is important to point out that all these materials were corroded in a mixed corrosion way, such as it has been reported previously by C. Cuevas et al. [10-17], and confirmed at least for AISI-316L for another authors [2,7]. The corrosion rate behavior of carbon steel with respect to that obtained for AISI-316L and AISI-316 is explained for the fact that the passivated layers of AISI-316L and AISI-316 are more compact and coherent due to their composition full of chromium, nickel and iron oxides [14,15], which provoked that the breakdown of the passive layer was more spaced, producing few sites of nucleation and localized corrosion, presenting a corroded surface of lower

pitting density than that of carbon steel. However, comparing Figure 2 to Figure 19, where electron images for AISI-316L and AISI-316 are presented for 60ºC in the later Figure, pits of AISI-316L and AISI-316 were much deeper and bigger, which led a major corrosion rate.

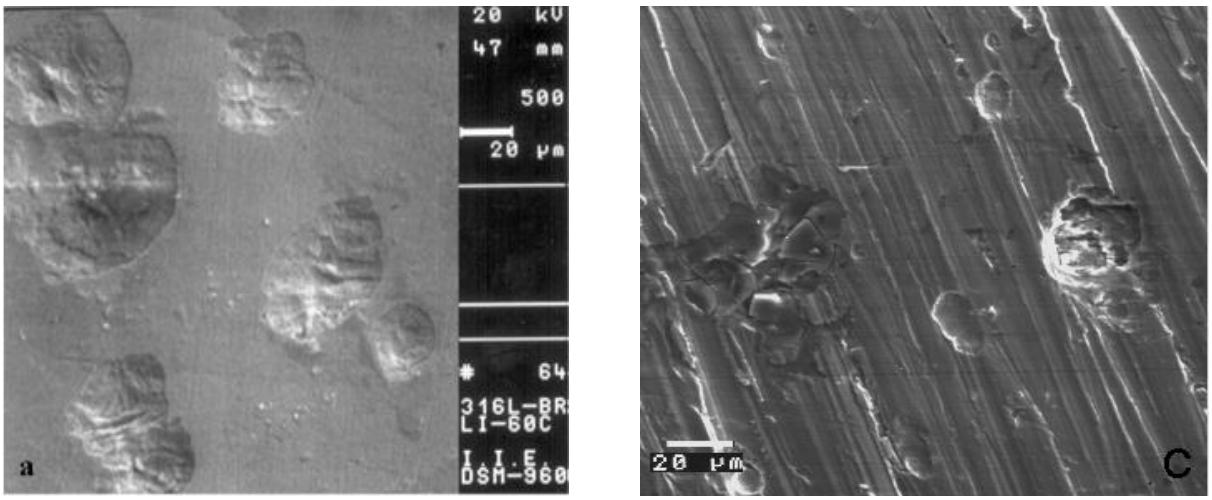

Figure 19. Electron images of SS-316L (a), and SS-316 (c) exposed to LiBr–H_2O (50% wt.) solution at 60ºC. Taken from C. Cuevas [14,15].

On the contrary, carbon steel was corroded in a localized-generalized way, observing a major pitting density over its surface, with much smaller and less profound pits, which caused a lower corrosion rate.

This behavior was due to the difference between the compositions of the passive layers of both types of materials, for which, the passive layer of carbon steel is formed to a great extent by iron oxide, but also by iron bromide, which was also identified. For AISI-316 and AISI-316L, it has been reported the presence of nickel and chromium bromides, additionally of iron bromides forming part of the corrosion products.

It is expected that these species as part of the corrosion products have profound effects on the corrosion behavior of metals, conferring to the passive layer a certain susceptibility to be broken and produce nucleation of pits, such as was observed in all the materials which corrosion rate is reported here. It is expected that the corrosion mechanism for materials containing chromium, nickel and iron alloying elements be different with respect to that almost containing only iron, nevertheless carbon steel presented a corrosion rate comparable to that obtained for stainless steel materials, which seems to indicate that iron oxide as passive layer responds competitively in terms of corrosion resistance under the specific environment conditions of the research presented in this paper. It is possible that in the case of carbon steel, the presence of just iron oxide and iron bromide produces good passivity conditions such as adherence or resistance removal capable to compete with alloys containing important amount of chromium, which has been considered one of the best resistance corrosion alloying element.

4. CONCLUSIONS

According to the experimental results obtained for carbon steel exposed to 50 wt-% lithium bromide aqueous solution at different temperatures, it is concluded as follows.

1.- Optical images of the microstructure of carbon steel revealed proeutectoid ferrite α plus pearlite phases. The pearlite consisted of ferrite interlaced with laths of cementite (Fe_3C). The ferrite grain shape was irregular, with a grain size about 10 μm.

2.- The morphological pattern of the corroded carbon steel surfaces was alike at all test temperatures, observing several pits through the samples and having an increment in the pitting density with temperature. The pits size was variable, from 2μm to 20 μm. It is observed that the sample at 25 ºC presented smaller amount of corrosion products than that at the higher temperatures, where the entire metallic surface was covered by corrosion products. EDS analysis showed a great amount of iron and bromide at the three temperatures, as an evidence of the formation of iron oxide as a primary corrosion product and iron bromide as a secondary corrosion product. From SEM analysis, it was concluded that carbon steel presents susceptibility to suffer pitting corrosion, especially when temperature increased.

3.- The polarization curves indicated that the temperature has an effect over the corrosion activity of the material, being more active the corrosion process when the temperature increases, hence the current density was becoming higher and E_{corr} became more active. At 25 and 80°C, the anodic curves showed only an active process, whereas at 60°C there was a current density limit of 0.03 mA/cm^2 observed approximately between 500 and 600 mV. The cathodic branches were analogous at all temperatures, showing a tendency to a limit current region after -200 mV, probably associated to oxygen diffusion, where the effect of mass transport or concentration polarization seemed to be present.

4.- At 25ºC, the current time series present some medium intensity anodic/cathodic transients together with stochastic oscillations in a sequential way, at 60ºC there were no transients, whereas at 80ºC, the current noise presented low-amplitude, high frequency stochastic oscillations accompanied with some significant transients. These transients were evidence for the nucleation of localized sites and/or the rupture and recovery of the passive film. At the two first temperatures, the current density tended to increase in time, but at 80ºC had an oscillatory behavior increasing at the beginning of the immersion, and decreasing afterward, which must be due to the thick passive layer formed at the higher temperature. This behavior was in agreement with the corrosion kinetics obtained from EN, where the corrosion rate at 60 and 80ºC was almost equal from the seven day of exposure.

5.- At 25 and 60ºC, the noise spectra indicated that noise impedance decreased with time of immersion at low frequency, indicating that corrosion rate increase in time, which was in agreement with the behavior of corrosion density obtained from the current time series. The range of impedance at low frequency for 60ºC was lower than that at 25°C, which means that the corrosion density is higher at the higher temperature. The spectral noise impedance at 80ºC, showed that at low frequencies the amplitude impedance was decreasing in time until 5 d, after that the amplitude increased, which is in agreement with the corrosion kinetics shown by EN data, which suggested an active condition at the beginning of the immersion and a passive condition afterward. From SN, a cyclic behavior in the slope

at 80ºC was seen, which means that the significant transients obtained from EN are alike in magnitude, then the noise magnitude decreases in frequency until making frequency independent, which could indicate that the corrosion phenomenon is repetitive along the immersion time, presenting pits of similar size and depth together with a generalized corrosion process, such as it was observed throughout the corresponding electron image.

6.- In general, the cumulative corrosion rate at the three studied temperatures increased with temperature. Corrosion rate at 80ºC was higher with respect to that at 60ºC until the 7^{th} day, subsequently; corrosion rate was similar at both temperatures. This behavior was explained thermodynamically considering that lithium bromide solution crystallized at 80ºC, and so, the amount of oxidizing species (Br) decreases, which induces a lower corrosion rate compared to that at 60ºC. Corrosion kinetics of several stainless steel (AISI-316, AISI-316L, AISI-304, AISI-310, AISI-310H, and AISI-321H) were compared to the corrosion kinetics of carbon steel at the same experimental conditions. Corrosion rate of carbon steel situated below corrosion rate of the two stainless steel with lower chromium content (AISI-316 and AISI-316L), and above corrosion rate of that stainless steel with higher chromium content (AISI-304, AISI-310, AISI-310H, AISI-321H). The major corrosion resistant of carbon steel compared to that of AISI-316 and AISI-316L was explained by the marked difference between the types of localized corrosion processes suffered for these materials. Finding a much lower pitting density in AISI-316L and AISI-316 with much deeper and bigger pits, which led a major corrosion rate. Also, the different composition of the passive layer of both materials (stainless steel and carbon steel) must have a significant effect on the characteristics such as adherence, thickness, and coherence. Such characteristics must be studied to elucidate the way in which the passive layer is acting to passivate the material and produce different type of broken and nucleation of pits.

7.- The results of the atomic absorption analysis demonstrated an increment of the concentration of iron with temperature. This behavior was also seen in the results of the corrosion rates from the electrochemical noise measurements. It was not possible to obtain some concentration of the other alloying elements present at low concentration in carbon steel.

ACKNOWLEDGMENTS

We wish to express our gratitude and thankfulness for the economical support for performing this research to PROMEP from the Public Education Secretary (SEP) of the Mexico Government through the project PROMEP-UAEMOR-EXB-01 granted to the first author.

References

1. F. A. Holland, *Appl. Therm. Eng.*, 20-9 (2000) 863
2. J. García-Antón, A. Igual-Muñoz, J. L. Guiñon and V. Pérez-Herranz, *Appl. Electrochem. J.*, 31 (2001) 1195
3. A.Igual-Muñoz, J. García Antón, J. L. Guiñon and V. Pérez-Herrans, *Corrosion*, 58-7 (2002) 560
4. H. Imai, Corrosion behavior of carbon steel in lithium bromide solution, Materials Science and Engineering (Master Course), 2001.

5. Guiñon J. L., J. García-Anton, V. Pérez-Herrans, and G. Lacoste, *Corrosion* 50-3 (1994) 240
6. Blasco-Tamarit, E., Igual-Muñoz, A., García-Antón, J, García-García D., *Corros. Sci*. 48 (2006) 863
7. Igual-Muñoz A., García Antón J., Guiñon J.L. and Pérez Herrans V, *Corrosion* 59-7 (2003) 606
8. D. García-García, J. García-Antón, A. Igual-Muñoz, E. Blasco-Tamarit, "Comparative Studies of the Corrosion Behavior of Welded and Non-Welded Duplex Stainless Steel in Aqueous LiBr Solutions Under Static and Dynamic Conditions," Proc. European Corrosion Congress 2005, paper no. P-218-F (Lisbon Portugal, Portuguese Materials Society).
9. Igual Muñoz A., J. García Antón, López Nuévalos S., J. Guiñón J.L, and Pérez Herranz V., *Corros. Sci*. 46 (2004) 2955
10. C. Cuevas-Arteaga, "Study of Corrosion Resistance of SS-304 Stainless Steel Exposed to Several Fluid Rates of a Lithium Bromide Aqueous Solution at 60 and 80°C," Proc. European Corrosion Congress 2005, paper no. P-B-13 (Lisbon Portugal, Portuguese Materials Society).
11. C. Cuevas Arteaga, F. Domínguez Crescencio, "Application of electrochemical noise technique to study the resistance corrosion of SS-316 stainless steel exposed in an aqueous lithium bromide solution," NACE 63th Annual Conference, paper no. 6414 (Houston, TX: NACE, 2006).
12. C. Cuevas-Arteaga, *Chem. Eng. Mexican Journal* 5 (2006) 27
13. C. Cuevas-Arteaga, J. Porcayo-Calderón, *Mat. Sci. & Eng. A* 435-436 (2006) 439
14. C. Cuevas-Arteaga, Ma. O. Concha-Guzmán, *Corros. Eng. Sci. and Tech*. 44-1 (2009) 57
15. C. Cuevas-Arteaga, F. Domínguez Crescencio, *Corrosion* 65 (2009) 748
16. Cuevas Arteaga, C, Balderrama-Martínez, A., Serna Barquera, S, Colín de la Cruz, XXIV Congreso de la Sociedad Mexicana de Electroquímica, Paper 247, Puerto Vallarta, Jalisco, México, June 2009.
17. Cuevas Arteaga Cecilia, Luna Brito Misael, XXIII Congreso Nacional de la Sociedad Mexicana de Electroquímica y 1ra. Reunión de Mexican Section of the Electrochemical Society, Paper 262, Ensenada Baja California, 2008, México.
18. ASTM G1 (1994), "Standard Practice for Preparing, Cleaning, and Evaluating Corrosion Test Specimens" ASTM International, West Conshohocken, PA, www.astm.org.
19. ASTM G31 (1995), "Standard Practice for Laboratory Immersion Corrosion Testing of Metals" ASTM International, West Conshohocken, PA, www.astm.org.
20. ASTM E407 (1999), "Standard Practice for Microetching Metals and Alloys", ASTM International, West Conshohocken, PA, www.astm.org.
21. J. G. Williams, C. R. Killmore, F. J. Barbaro, J. Piper and L. Fletcher, High Strength ERW Linepipe Manufacture in Australia, Materials Forum, 1996, 20, 13-28
22. J.- C. Cuevas-Arteaga, J. Castrellon-Uribe, A. Trujillo- Estrada, *ECS Transactions* 3-24 (2007) 33
23. W. Skinner, Br. *Corros. J*. 22-3 (1987) 172
24. A.Rahmel, *Mater. Sci. Eng.* 87 (1987) 345
25. Carmel B. Breslin, Amy L. Rudd, *Corros. Sci*. 42 (2000) 1023
26. R. Cottis, S. Turgoose, in B.C. Syrett (Ed), Electrochemical Impedance and Noise, NACE, Corrosion Testing Made Easy, Houston, 1999.
27. J.M. Sanchez-Amaya, R. A. Cottis, F.J. Botana, *Corros. Sci.* 47 (2005) 3280
28. F. Mansfeld, L.T. Han, C.C. Lee, C. Chen, G, Zhang and H. Xiao, *Corros. Sci.* 39-2 (1997) 255
29. F. Mansfeld, Z. Sun, E. Speckert, C.H. Hsu, "Electrochemical Noise Analysis (ENA) for Active and Passive Systems," NACE 57th Annual Conference, Paper no. 418 (Houston, TX: NACE, 2000).
30. Scully John R., Electrochemical, Corrosion Tests and Standards: Application and Interpretation", Robert Baboian (ed.), ASTM Manual Series: MNL 20, chapter 7, pp. 75-90, 1995.
31. Mansfeld F., C.C. Lee and G. Zhang, *Electroch. Acta* 43, 3-4 (1998) 435
32. Zhou X. Y., S.N. Lvov, X.J. Wei, L.G. Benning, D.D. Macdonald, *Corros. Sci*. 44 (2003) 841

33. ASTM G102 (1994), "Standard Practice for calculation of corrosion rates and related information" ASTM International, West Conshohocken, PA, www.astm.org.